Acta Polytechnica **64**(1):25–33, 2024
https://doi.org/10.14311/AP.2024.64.0025

Published by the Czech Technical University in Prague

ASSESSING THE EFFICACY OF FLAT-PLATE SOLAR COLLECTORS USING NANOFLUIDS IN THE CLIMATIC CONTEXT OF KIRKUK CITY, IRAQ

Adnan M. Hussein, Hussein Hayder Mohammed Ali, Zahraa H. Mohammed Ali*

Northern Technical University, Technical college of Engineering, 36001 Kirkuk, Iraq

* corresponding author: zahraa.h.m@ntu.edu.iq

Abstract. Solar energy is a key renewable energy source. Research and development have focused on enhancing the heat transfer coefficient, heat gain, and practical efficiency of solar systems. The aim of this study is to evaluate the performance of a flat solar panel collector using a nanofluid under conditions in the city of Kirkuk/Iraq, 35° latitude and 45° longitude, in terms of practical calculation of thermal efficiency. The study included making two solar collectors, one traditional and the other improved using a nanofluid (CuO). The CuO/Water nanofluid was prepared with a volumetric concentration of 0.25 % by mechanical mixing and then ultrasonic mixing to homogenise the particles and eliminate the agglomerations that form inside the fluid. Practical testing was conducted for the two solar collectors, one using distilled water and the other using the nanofluid, during four months (January, February, March, and April) of the year 2023. The experiments revealed that the efficiency progressively improves from 9:00 a.m. to 1:00 p.m. This increase is attributed to solar radiation's decreasing intensity post 12:00 p.m., while thermal storage and minimised thermal losses continue to contribute. After 2:00 p.m., the efficiency dwindles due to the declining solar radiation intensity. The practical efficiency of a 0.25 % nanofluid (CuO) attains its zenith at a mass flow rate of 0.015 L s^{-1}. Higher mass flow rates enhance heat transfer within fluid-filled tubes. The collector efficiency at this flow rate ranges from 31.66 % in January to 44.44 % in April.

Keywords: Nanofluids, flat-plate solar collectors, solar energy, Nusselt number, Reynolds number.

1. Introduction

Globally, energy sources can be divided into two main groups: fossil fuels and renewable energy sources. Fossil fuels, used extensively since the beginning of the industrial revolution, are recognised as significant contribution to environmental degradation. Notable examples include coal, oil, and natural gas. Conversely, renewable energy, inherently replenished by nature, offer cleaner alternatives devoid of harmful pollutants [1].

Makhzom et al. based their research on actual measured data collected over long periods by the monitoring and control systems of the power plants in question. As a result, the following CO2 emission factors that are shown below can be regarded as a gauge of the environmental status of Libya's power industry sector. The study's technique can be applied to other industries or even to estimate emission factors for different types of air pollution outside of the power industry [2].

Among the essential renewable energy types are solar, wind, geothermal, ocean wave, and biomass, solar energy, particularly, holds a paramount importance. In the present day, solar flat-plate collectors (FPCs), a renewable energy conversion system, are becoming increasingly popular for providing hot water and hot air in both the domestic and industrial sectors. This limitation stems from the fact that the upper limit of nonconcentrated solar radiation energy is around 5.3 % at an ambient temperature of 300 K. The issue of low efficiency has been a focal point in both historical and recent theoretical and experimental research efforts. Despite the efficacy of evacuated tube collectors for water heating, their high cost persists as a drawback. Solar collectors generally function by transferring solar heat to a working fluid, such as water, in the context of solar water heating. The widely employed flat plate-solar collector is a form of heat exchanger, harnessing solar radiation's energy for heating fluids, such as water or air. Typically, operational at temperatures around 100 °C, these collectors use air or water as heat transfer mediums [3].

Solar radiation heats up the absorbent material, using a suitable working fluid to cool the plate and extract the accumulated heat. This fluid circulates through passages connected to the plate, known as risers. A key challenge with solar water heaters, as with other energy conversion devices, is thermal efficiency. Hence, the research in this field is focused on improving thermal efficiency and improve the performance of flat-plate solar water heaters (FPSWHs). Strategies to improve heat transfer include active methods requiring an external input and passive methods without any external influence. The use of a nanofluid as a working fluid in a heat exchanger is a means of

improving heat transfer efficiency [4].

While numerous studies have explored nanofluids in heat exchangers, the effects of nanofluids on the thermal performance of flat-plate solar collectors have not been properly investigated [5]. A comparative experimental study by Tong et al. [6] in Gwangju, South Korea, demonstrated that using multi-walled carbon nanofluids (MWCNT) increase the flat-plate solar collector efficiency to 87 %, while water usage reduced the efficiency to 62 %. Similarly, Sadeghzadeh et al. [7] investigated a flat solar collector's thermal performance using TiO_2 (20 nm)/aqueous nanofluids. Their findings revealed that the thermal efficiency varied based on concentration, input temperature, and flow rate.

Choudhary et al. [8] conducted an experimental study to improve the efficiency of a planar solar collector using ZnO nanofluids. Their results indicated that thermal efficiency increases with flow rate and exit temperature, with a maximum efficiency of 69.24 % observed. Moravej et al. [9] studied rutile TiO_2 aqueous nanofluids in flat-plate solar collectors and discovered that the efficiency improved with increased solar radiation or flux rate. Notably, the introduction of nanoparticles led to efficiency gains of up to 33.54 % for various nanoparticle concentrations.

In essence, these studies highlight the potential of nanofluids to improve the performance of flat-plate solar collectors, showing a potential advances in thermal efficiency and broader applications in sustainable energy systems.

Omar et al. (2020) [10] investigated the optimisation of thermal performance in a flat-plate solar collector using a hybrid nanofluid. This study explored various concentrations of hybrid nanoparticles with the use of Tween 80 (Tw-80) as a surfactant. The efficiency of the flat-plate solar collector was evaluated at different flow rates (2, 3, and 4 litres per minute), by ASHRAE 93-2010 guidelines. The introduction of a hybrid nanofluid at a flow rate of $4\,\mathrm{l\,min^{-1}}$ significantly improved the efficiency of the most thermally efficient collector by up to 85 %. Fluid outlet temperatures increase with increasing nanoparticle concentration, indicating improved thermal energy gain. Nirmala [11] conducted an experimental study on a horizontal solar collector aimed at efficiency improvement. By maintaining a 2cm gap between the glass and the absorbing plate, the researcher found that doubling the glass plates' arrangement doubled the efficacy of the flat-solar collector as compared to a single glass plate. Zarda et al. [12] studied the thermal performance of flat-plate solar collectors (FPSCs), which are known for their cost-effectiveness, simplicity, and ease of use. They focused on improving the efficiency of these collectors by introducing diamond/H_2O nanofluids, a type of fluid containing tiny diamond particles. To assess the impact of these nanofluids on the collector performance, the researchers conducted a numerical analysis using ANSYS/FLUENT software, simulating real-world scenarios in Iraq's hot climate. This choice of location is significant as it mimics the conditions in regions with high temperatures and intense solar radiation. One key observation was the variation in collector temperature throughout the day, with a decrease in temperature occurring as solar intensity decreased post-midday. This finding highlights the importance of understanding how collectors perform under changing solar conditions. The most remarkable result was the significant improvement in collector efficiency. The highest thermal efficiency achieved was 68.90 %, and this was accomplished with a 1 % concentration of diamond nanoparticles in water as the nanofluid. This represented a substantial 12.2 % improvement compared to using plain water as the heat transfer fluid. The choice of nanofluid concentration proved to be critical. The 1 % nanofluid concentration outperformed other concentrations due to changes in the nanofluid's physical properties and a notable increase in thermal conductivity. This highlights the significance of selecting the right nanofluid for optimising the collector performance.

Furthermore, the study highlighted the direct relationship between the solar radiation intensity and the outlet temperature from the solar collector. This connection was most pronounced around 12:30 p.m., coinciding with the collector's peak efficiency. This finding only proves the importance of aligning the collector operation hours with periods of higher solar intensity to maximise the efficiency. Okonkwo et al. (2020) [14] carried out an experimental investigation on a $1.51\,\mathrm{m^2}$ flat solar collector using single and hybrid nanofluids (Al_2O_3 and Al_2O_3-Fe) mixed with water. At concentrations of 0.1 % and 0.2 %, the nanofluid (Al_2O_3) increased thermal efficiency by 2.16 %, while the hybrid nanofluid decreased efficiency by 1.79 % compared to water. Hybrid nanofluids showed a 6.9 % improvement in efficiency compared to single nanofluids. Alklaibi et al. [15] tested a planar solar collector and found that introducing a 1 % concentration of nano-diamond fluid to water improved the collector's efficiency by 69.8 %. Entropy generation values ranged from 5.541 % to 5.725 % with the use of nanofluids. Akram et al. (2021) [16] investigated the performance of flat collector solar panels using carbon and metal oxide-based nanofluids. Stable nanofluids were created using covalently functional carbon nanoparticles and non-covalently functionalised metal oxides. The study demonstrated improvement of conductivity in nanofluids, with nanoparticles, such as f-GNPs, SiO_2, and ZnO, by increasing concentrations by 25.68 %, 11.49 %, and 15.44 %, respectively. Farhana et al. [17] studied the effects of nanocellulose (CNC) nanofluids on improving flat plate solar collector efficiency. By using 0.5 % CNC and 0.5 % Al_2O_3 nanofluids, the efficiency improved by 2.48 % and 8.46 %, respectively. The study also observed temperature-dependent increases in thermal conductivity and decreases in viscosity of the nanofluids. In essence, nanofluids show a promis-

Matter	Density [kg m^{-3}]	Specific heat [J kg^{-1} K^{-1}]	Thermal conductivity [W m^{-1} K^{-1}]	Viscosity [Pa s]
Water	997.13	4 179	0.605	0.00089
CuO	6 302	959.1	76.5	–
0.25 % CuO/Water	1 010.263	4 128.786	0.619014	0.00086

TABLE 1. Thermal characteristics of water and nanoparticles [13].

ing potential for improving the efficiency of flat-panel solar collectors.

2. EXPERIMENTAL SETUP

This study involves a test setup with two flat solar collectors: the first collector operates with pure water, while the second uses nanofluids containing 0.25 % volumetric concentration of copper oxide mixed with water as the base liquid. The thermal characteristics of the water and nanoparticles are shown in Table 1. The collectors are equipped with temperature sensors to monitor the inlet temperature, outlet temperature, glass surface temperature, and absorber plate temperature. Parameters like volumetric water flow, solar radiation intensity on the collector, and wind speed are also measured.

Experimental investigations were conducted to assess practical efficiency. The study compared the performance of the solar collector using pure water with that of using nanofluid containing 0.25 % volumetric concentration of copper nanoparticles in water as the base fluid. The experiments were conducted from 9:00 a.m. to 5:00 p.m. at day, with volume flow rates of 0.0089, 0.012, and 0.015 l/s to determine the solar collector's optimal performance parameters. A visual representation of the test configuration can be seen in Figure 1.

FIGURE 1. The experiment setup.

2.1. FLAT SOLAR COLLECTOR

The system consists of a square-shaped aluminium enclosure measuring 1 m by 1 m. The outer portion comprises three layers of plastic panels, while the inner layer is made of aluminium, with a 5 cm gap between them. Insulating glass wool is placed within the gap, topped by a 4 mm thick layer of transparent glass cover. This thickness was selected to suit the substantial cross-sectional area of the unit, safeguarding it from potential breakage and weather conditions. The design allows for optimal energy absorption from above, allowing unobstructed solar radiation penetration while simultaneously minimising heat loss from the structure's surface. The collector is thermally insulated from its base and sides. The scheme of the flat solar collector is shown in Figure 2. For the second collector variant, the preparation of nanofluid (CuO/water) was achieved by mechanical mixing using an electric mixer. This process ensured uniform suspension and dispersion of the nanoparticles within the water medium. The solar collector is constructed using copper tubes measuring 0.85 m in length, with the following specifications:

- Header inner diameter: 22.5 mm, thickness: 1 mm.
- Riser inner diameter: 9.5 mm, thickness: 1.5 mm.

To prevent any heat dissipation from the storage tanks to the surroundings, insulation was applied to the internal surfaces of the setup using two layers of Armaflex insulation material. The integration of the solar collectors into the system was achieved by using plastic tubes with a diameter of 1/2 in. These tubes were used as conduits for facilitating the flow of both water and nanofluids. Additionally, the system was equipped with a range of connections and valves designed to regulate the fluid flow effectively.

To ensure the required circulation, two vertical pumps with a power rating of a quarter horsepower and a minimum height of 2.5 m were used. One pump was dedicated to conveying the nanofluid from its designated tank to the nanofluid test system's flatbed solar collector. The second pump was responsible for pumping the purified water from its storage tank to the flatbed solar collector in the water test system.

In addition, the system was equipped with a specialised instrument designed to precisely measure the flow rate of both water and nanofluids. The components of the test system were mounted on two metal bases, one serving as the mount for the fluid tank,

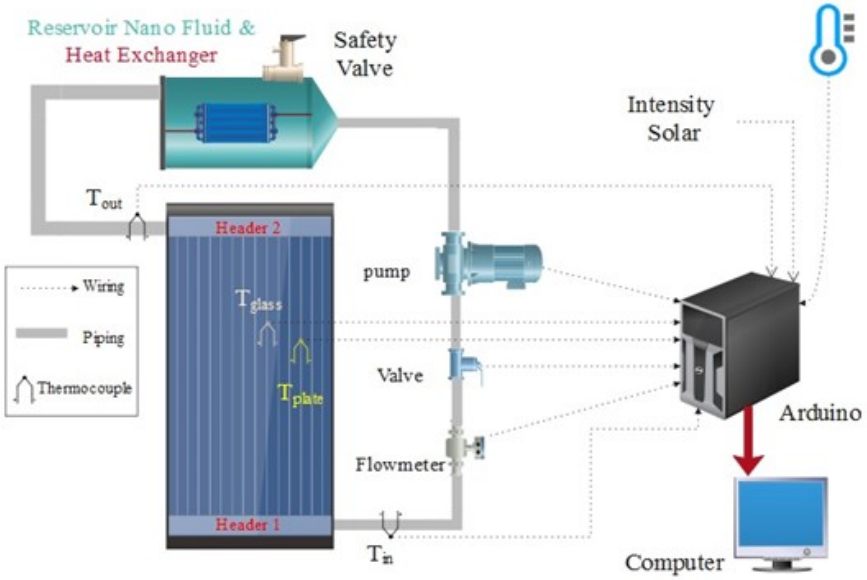

Figure 2. A scheme of the flat solar collector.

and the other supporting the flat solar collectors of both systems (water and nanofluids). Two additional bases were designated for accommodating the flowmeters and digital scales. Thermocouples were used for measuring the temperatures of the system.

2.2. Measuring devices of the solar collector and calibrations

For monitoring the flow rates of both pure water and nanofluids, a water flow sensor (YF, S201) with a functional range of 1–30 L min^{-1} and a maximum water pressure tolerance of 1.75 MPa was employed. These flow sensors were carefully positioned according to the configuration shown in Figure 2.

To measure the temperature of the fluid within the primary and secondary solar collectors, a device was developed to record the temperature, flow, and radiation intensity. This device operates on an Arduino chip. Specifically, the Arduino UNO variant was chosen for its compatibility with the variables needed for this study. It has 12 input and output points and uses an external memory card (external memory) for permanent data retention.

In each of the test systems, one using pure water and the other employing nanofluid, seven data points are captured: inlet temperature, outlet temperature, absorber plate temperature, cover glass temperature, ambient temperature, flow rate, and radiation intensity. Readings are recorded on an hourly basis, and the results are stored on a memory drive, as depicted in Figure 2.

For temperature measurements, four digital Arduino type [K] temperature sensors and four analogue Arduino system connected (NTC) temperature sensors were used. These sensor pairs were placed as follow:

Temperature measurements were taken during the experiment to determine the input and output temperatures of the clean water as it transitions from the main system to the flat-plate solar collector. Two thermal sensors were placed at both ends of the tube (header). Similarly, for the nanofluid, its input and output temperatures as it flows from the main system to the flat-plate solar collector are measured using two thermal sensors at both ends of the tube (header).

On the absorber plate, temperature monitoring involves installing two thermal sensors for each of the systems. This arrangement allows for accurate measurement of the surface temperature of the absorber plate. Similarly, two thermal sensors are positioned on the glass cover. This arrangement allows measuring the surface temperature of the glass cover of both.

Furthermore, ambient temperature readings are obtained by placing thermal sensors in the proximity of both experimental systems. This approach ensures an accurate measurement of the surrounding temperature conditions, improving the comprehensiveness of the collected data.

3. Theoretical methodology

Flat-plate solar water collector performance (useful energy): The usable energy production of a flat-plate solar water collector in steady state is [18, 19]:

$$Q_{\mathrm{u}} = \dot{m} \times C_{p_{nf}} \times (T_{\mathrm{w,co}} - T_{\mathrm{w,ci}}), \qquad (1)$$

where m is the fluid mass flow rate [kg s^{-1}], $C_{\mathrm{p,nf}}$ is the nanofluid specific heat $\left[\mathrm{kJ\,(kg\,K)^{-1}}\right]$, $T_{\mathrm{w,ci}}$ and $T_{\mathrm{w,co}}$ [K] are the temperatures of the fluid at the inlet and the outlet of the solar collector, respectively.

The hourly efficiency, η_{sc}, for the flat plate solar water collector is [20]:

$$\eta_{\mathrm{sc}} = \frac{\int_{t_1}^{t_2} Q_{\mathrm{u}} \mathrm{d}t}{A_{\mathrm{sc}} \int_{t_1}^{t_2} I(t) \mathrm{d}t} \times 100\,\%, \tag{2}$$

where $I(t)$ is the instantaneous solar radiation intensity [W m^{-2}] and A_{sc} is the flat-plate solar water collector area [m^{-2}].

4. Results and discussion

This section offers a comprehensive analysis of the results obtained from the conducted tests on the flat solar collectors. These tests were designed to improve various aspects, such as the heat transfer coefficient, heat gain, power, and operational efficiency, of a solar collector. The initial case involved using water as a benchmark for reference, aimed at quantifying the percentage improvement in the efficiency of the flat-plate solar collector.

Subsequently, the investigation progressed to the second case, where a nanofluid with a 0.25 % concentration of (CuO) nanoparticles was introduced. Different flow rates, specifically 0.0089, 0.012, 0.018 L s^{-1}, were considered. Additionally, numerical simulations of the same system, conducted under comparable conditions, were performed using pure water and copper nanoparticles at a 0.25 % concentration. The subsequent comparison of these simulation results allowed for the assessment of their relative effectiveness and performance.

Figure 3 illustrates the relationship between solar radiation and the average daily time over a span of four months (January, February, March, and April). Across these four months, a discernible pattern emerges in the intensity of solar radiation, marked by a consistent rise from 9:00 a.m. to midday. This phenomenon can be attributed to the perpendicular alignment of the sun's rays with the Earth's surface, resulting in a higher radiation absorption.

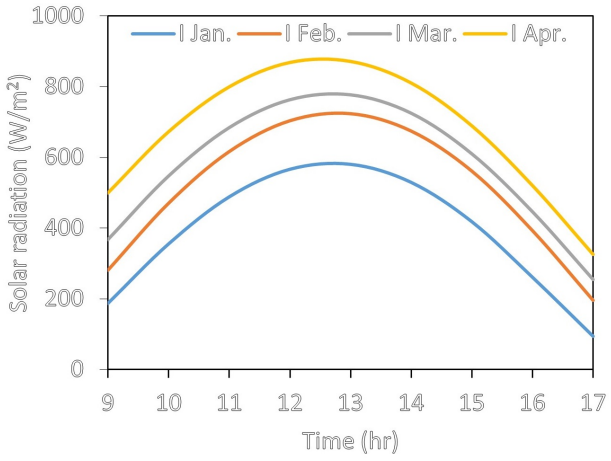

Figure 3. The intensity of solar radiation with the average time for the four months of 2023, Kirkuk/Iraq.

The trend continues as the solar radiation reaches its zenith at noon, achieving a peak intensity of 580 W m^{-2} in January. Subsequent months show even higher peaks, with February, March, and April reaching 723 W m^{-2}, 777 W m^{-2}, and 871 W m^{-2}, respectively, at 12:00 a.m. This is because the sunrays are most directly overhead during this time.

However, as the afternoon progresses, the solar radiation intensity starts to decrease. This decline corresponds to the changing angle of the sun as it moves away from the perpendicular position to the Earth's surface, ultimately resulting in decreased radiation intensity.

Figure 4 shows the correlation between air temperature and the progression of time across the four months (January, February, March, and April). The graph reveals significant fluctuations in air temperature during this period. Notably, there is a discernible trend of rising temperatures as we transition into the summer months.

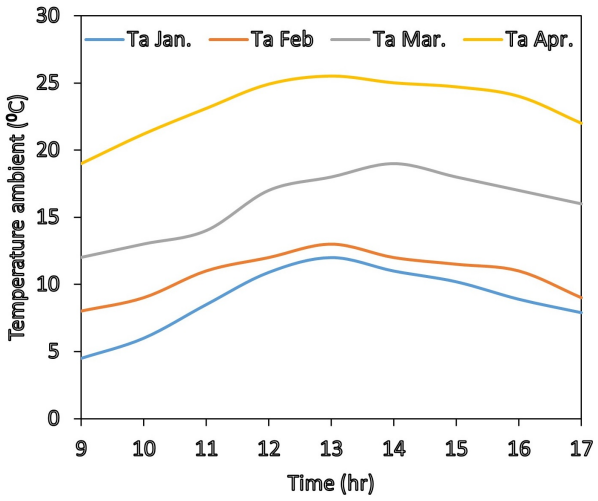

Figure 4. Air temperatures for the four months of 2023 Kirkuk/Iraq.

This relationship can be attributed to the increasing influx of solar radiation reaching the Earth's surface. As solar radiation intensifies, it contributes to elevated air temperatures over extended periods, particularly evident during the summer-preceding month of April. In April, the temperature peaked at 25.5 °C in the afternoon, demonstrating the warming effect of intensified solar radiation as summer approaches.

Figure 5 illustrates the relationship between wind speed and the current month (January, February, March, and April). The graph demonstrates the dynamic nature of wind speed as it varies throughout the day. Notably, the highest wind speeds were observed around noon across the four months. April had the highest wind speeds due to the increased temperatures characteristic of that time of year.

In April, the maximum wind speed reached an impressive 13.2 m s^{-1} at 5:00 p.m. in the afternoon. Conversely, the month of January had the lowest wind speed, nearly approaching zero. This variation of wind speed highlights the correlation between wind speed

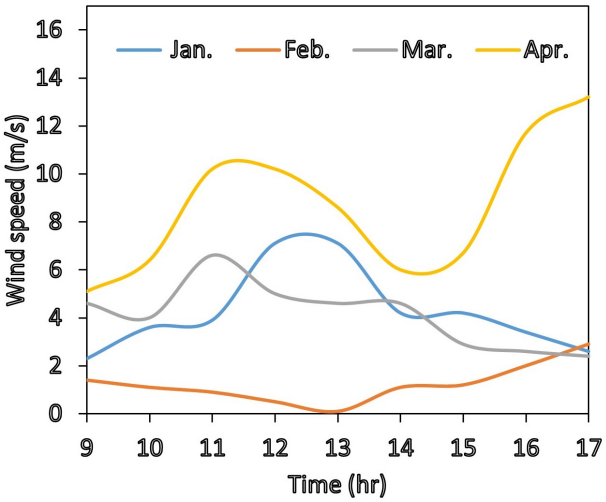

Figure 5. Wind speed over time for the four months of 2023, Kirkuk/Iraq.

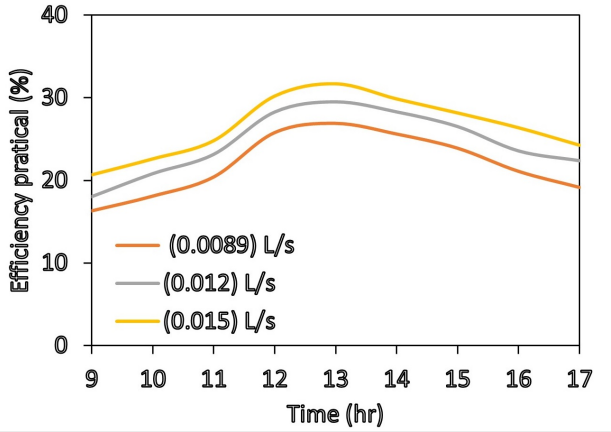

Figure 6. Thermal efficiency with time at different volume flow rates of nanofluid (CuO) at a concentration of 0.25 % for January 2023, Kirkuk/Iraq.

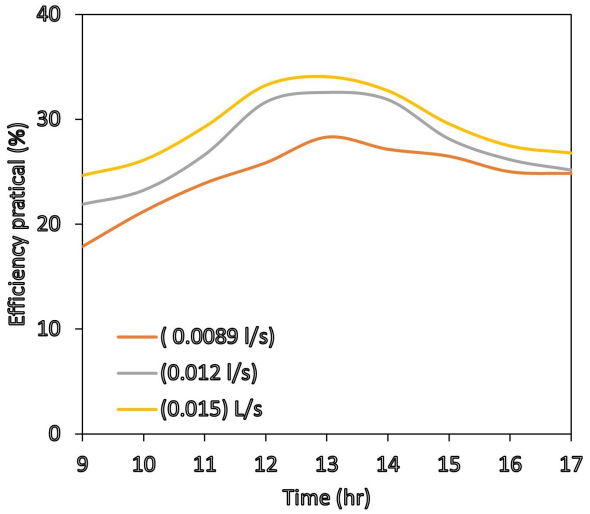

Figure 7. Thermal efficiency over time at different volume flow rates of nanofluid (CuO) at a concentration of 0.25 % for February 2023, Kirkuk/Iraq.

and temperature fluctuations, as well as the overall climatic conditions during these months.

The relationship between efficiency and time for different volume flow rates of 0.0089, 0.012, and 0.015 $\mathrm{L\,s^{-1}}$ of the nanoparticle fluid (CuO) at a concentration of 0.25 % can be seen from the thermal efficiency values in Figures 6 to 9. Notably, the efficiency demonstrated an upward trend from 9 a.m. to 1:00 p.m., with outcomes suggesting a direct correlation between the solar radiation intensity and collector efficiency. This effect is attributed to the thermal storage capacity of the solar collector and the atmospheric conditions.

While solar radiation intensity decreases post-noon, the efficiency continues to rise until 1:00 p.m., due to the minimised thermal losses. However, after 2:00 p.m., as solar radiation intensity further decreases, the collector's efficiency begins to decrease until around 5 p.m. The data presented in Figure 6 for January indicate that the highest efficiency was achieved at the highest volume flow rate of 0.015 $\mathrm{L\,s^{-1}}$. This notable efficiency increase is due to the increased volume flow rate, which disrupts adjacent layers within the tubes, thereby improving the heat transfer from the tube's surface to the fluid's interior.

For the volume flow rate of 0.015 $\mathrm{L\,s^{-1}}$, the efficiency reached 31.66 % at 1 p.m. compared to 29.52 % for 0.012 $\mathrm{L\,s^{-1}}$ and 26.91 % for 0.0089 $\mathrm{L\,s^{-1}}$. The increase in efficiency for the flow rate of 0.015 $\mathrm{L\,s^{-1}}$ compared to 0.012 $\mathrm{L\,s^{-1}}$ was 7.24 % and 17.65 % for 0.0089 $\mathrm{L\,s^{-1}}$. Similar trends were observed for February, where the highest efficiency was observed for the highest volume flow rate of 0.015 $\mathrm{L\,s^{-1}}$, as can be seen in Figure 7. With the increase in volume flow rate, the disruption of adjacent layers within the tubes becomes more pronounced, leading to an improved heat transfer from the tube surface to the fluid. This effect is evident in the recorded efficiencies. In the case of February, the highest efficiency was observed at a volume flow rate of 0.015 $\mathrm{L\,s^{-1}}$, reaching 34.06 % at 1:00 p.m. Comparatively, efficiencies for volume flow rates of 0.012 $\mathrm{L\,s^{-1}}$ and 0.0089 $\mathrm{L\,s^{-1}}$ were 32.55 % and 28.32 %, respectively. The efficiency increased by 4.54 % when the flow rate changed from 0.012 $\mathrm{L\,s^{-1}}$ to 0.015 $\mathrm{L\,s^{-1}}$, and by 20.26 % when it changed from 0.0089 $\mathrm{L\,s^{-1}}$ to 0.015 $\mathrm{L\,s^{-1}}$. In March, the highest efficiency was once again achieved for the highest volume flow rate of 0.015 $\mathrm{L\,s^{-1}}$. This trend persisted because as the volume flow rate increases, the efficiency also tends to increase. Specifically, at 1:00 p.m., the efficiency reached 39.58 % for a volume flow rate of 0.015 $\mathrm{L\,s^{-1}}$ compared to 37.02 % for 0.012 $\mathrm{L\,s^{-1}}$ and 32.03 % for 0.0089 $\mathrm{L\,s^{-1}}$. The efficiency increased by 6.9 % when the flow rate changed from 0.012 $\mathrm{L\,s^{-1}}$ to 0.015 $\mathrm{L\,s^{-1}}$, and by 23.57 % when it changed from 0.0089 $\mathrm{L\,s^{-1}}$ to 0.015 $\mathrm{L\,s^{-1}}$, details can be seen in Figure 8.

Lastly, Figure 9 demonstrates the results for April, where the highest efficiency was achieved with the largest volume flow rate of 0.015 $\mathrm{L\,s^{-1}}$. At 1:00 p.m.,

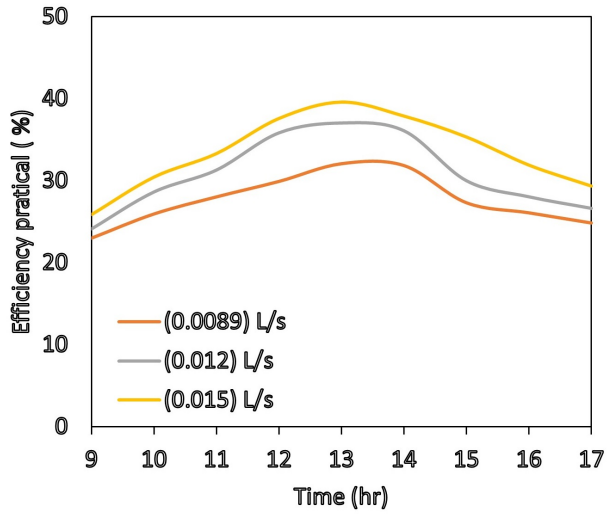

FIGURE 8. Thermal efficiency over time at different volume flow rates of nanofluid (CuO) at a concentration of 0.25 % for the month of March 2023, Kirkuk/Iraq.

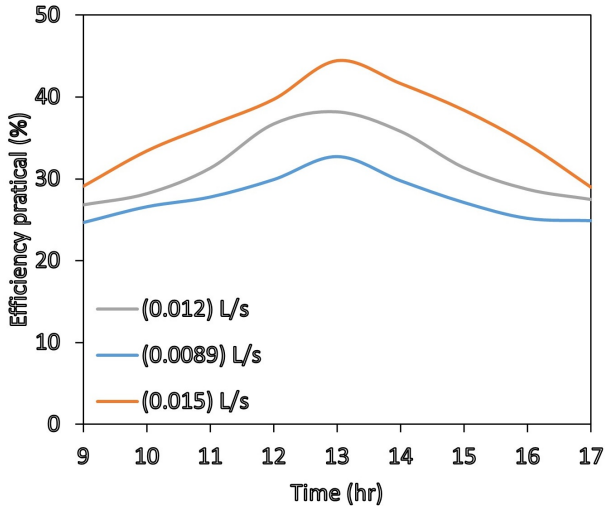

FIGURE 9. Thermal efficiency over time at different volume flow rates of nanofluid (CuO) with a concentration of 0.25 % for the month of March 2023, Kirkuk/Iraq.

the efficiency for this flow rate reached 44.44 %.

The subsequent Figures 10–13 illustrate the correlation between thermal efficiency and time rate at a constant volume flow rate of $0.015\,\mathrm{L\,s^{-1}}$. These figures pertain to the month of January and involve both the pure water and the nanofluid containing CuO nanoparticles at a concentration of 0.25 %. The observed trend indicates that the efficiency progressively increases from 9 a.m. to 1 p.m., due to the increasing solar radiation intensity. Conversely, it decreases between 1 p.m. and 5 p.m. due to the decreasing intensity of incident solar radiation for both scenarios (pure water and CuO nanofluid).

As can be concluded, the depicted figures highlight the highest efficiency in the case of the CuO nanofluid. The results indicate that the physical properties of

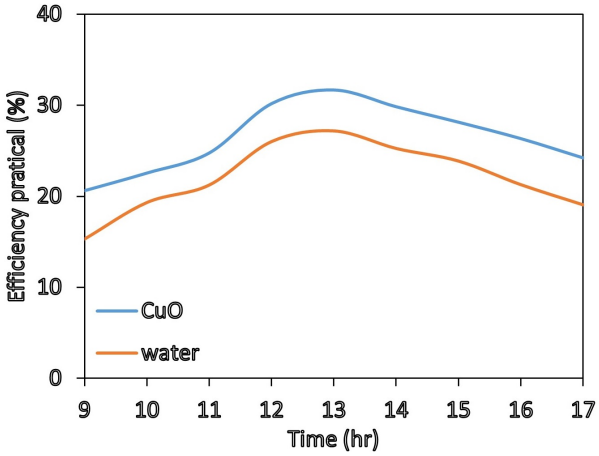

FIGURE 10. Thermal efficiency over time for a volume flow rate of $0.015\,\mathrm{L\,s^{-1}}$ for pure water and nanofluid (CuO) at a concentration of 0.25 % for January 2023 Kirkuk/Iraq.

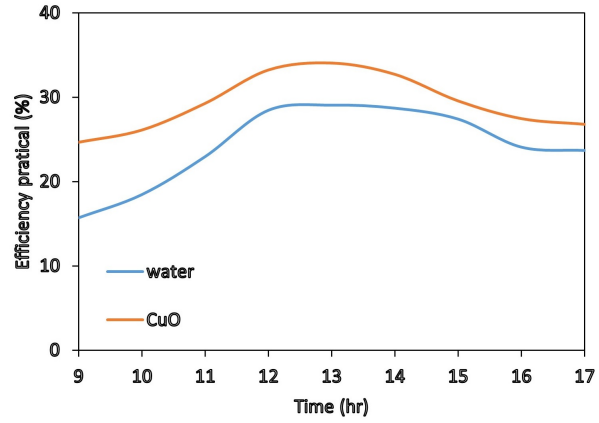

FIGURE 11. Thermal efficiency over time for a volume flow rate of $0.015\,\mathrm{L\,s^{-1}}$ of pure water and nanofluid (CuO) at a concentration of 0.25 % for February 2023 Kirkuk/Iraq.

the fluid (pure water) are enhanced by the addition of nanoparticles. This improvement involves increasing the fluid's thermal conductivity, which enhances heat transfer between the solar collector's tube wall and the fluid. The presence of nanoparticles in the fluid also promotes turbulent movement, further improving heat transmission between the tube wall and the fluid within the collector.

As can be seen from Figure 10, which shows the results from January, the efficiency of the CuO nanofluid in the solar collector reached 31.66 % at 1:00 p.m., while pure water reached an efficiency of 27.18 %. That is an increase of 16.48 % compared to the CuO nanofluid with pure water. Similarly, in February, the efficiency of the CuO nanofluid reached 34.06 % at 1:00 p.m., as compared to pure water's efficiency of 29.07 %.

Similarly, as can be seen from Figure 11, in February, the measured efficiency of the CuO nanofluid reached 34.06 % at 1:00 p.m. in contrast to the efficiency of

pure water, which reached 29.07 %. This illustrates a significant increase in efficiency of 17.16 % attributed to the CuO nanofluid.

In March, the efficiency of the CuO nanofluid within the solar collector reached 39.58 % at 1:00 p.m., while pure water reached an efficiency of 31.23 %, as shown in Figure 12. In April, the efficiency of the CuO nanofluid in the solar collector reached at 44.44 % at 1:00 p.m., while pure water reached an efficiency of 32.61 %, as shown in Figure 13.

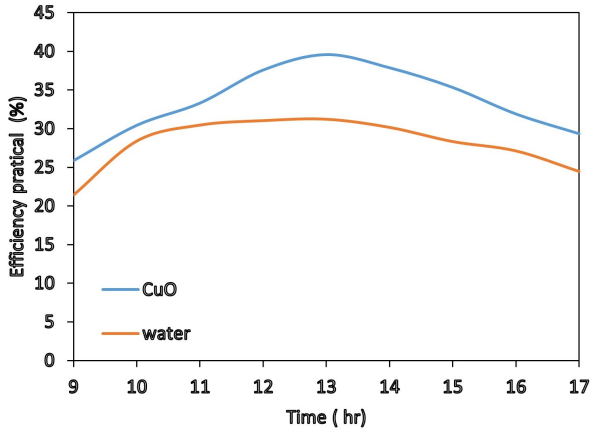

Figure 12. Thermal efficiency over time for a volume flow rate ($0.015\,\mathrm{L\,s^{-1}}$) for pure water and nanofluid (CuO) at a concentration of 0.25 % for the month of March 2023 Kirkuk/Iraq.

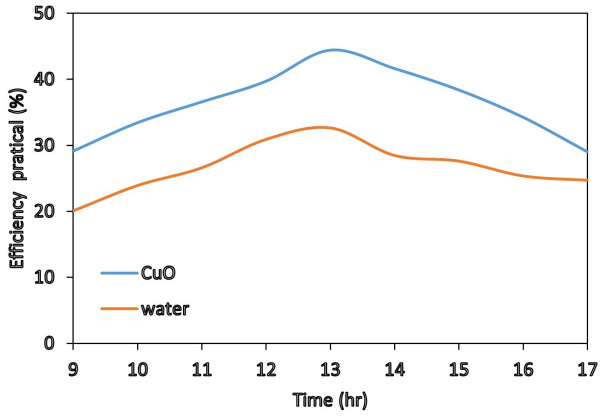

Figure 13. Thermal efficiency over time for a volume flow rate of $0.015\,\mathrm{L\,s^{-1}}$ of pure water and nanofluid (CuO) at a concentration of 0.25 % for the month of April 2023 Kirkuk/Iraq.

It's important to note from the aforementioned Figures 10–13 that the highest thermal efficiency was consistently observed with the highest volume flow rate ($0.015\,\mathrm{L\,s^{-1}}$) during April. This is due to the heightened solar radiation intensity during this specific month compared to the others under consideration.

5. Conclusions

From the experimental results, it can be concluded that the efficiency of the solar collector displays an upward trend from 9:00 a.m. to 1:00 p.m. This trend suggests that despite the decline in solar radiation intensity post-noon, the efficiency continues to increase until 1:00 p.m. This effect is attributed to the thermal storage of the solar collector and its surroundings, leading to reduced heat losses – the dissipation of heat from the collector to the external environment.

Around 2:00 p.m., the efficiency of the collector starts to decrease due to the lower solar radiation intensity during that period. The peak efficiency of the nanofluid (CuO) at a concentration of 0.25 % was achieved with the highest mass flow rate ($0.015\,\mathrm{L\,s^{-1}}$). This outcome is linked to the fact that a greater mass flow rate disrupts the adjacent layers within the tubes, resulting in improved heat transfer from the tube's surface to the fluid.

For reference, at a mass flow rate of (0.015) litres per second, the measured collector efficiency was 31.66 %, 34.06 %, 39.58 %, and 44.44 % in the months of January, February, March, and April, respectively.

References

[1] S. Tarik Ahmed, H. Hayder Mohammed Ali. Experimental investigation of new design of solar water distillation coupled with flat plate solar water collector. *The Iraqi Journal for Mechanical and Material Engineering* **20**(3):193–207, 2019. https://doi.org/10.32852/iqjfmme.v20i3.512

[2] A. A. Makhzom, A. M. Eshdok, Y. F. Nassar, et al. Estimation of Co_2 emission factor for power industry sector in Libya. In *2023 8th International Engineering Conference on Renewable Energy & Sustainability (ieCRES)*. IEEE, 2023. https://doi.org/10.1109/ieCRES57315.2023.10209528

[3] J. Zhao, Y. Yuan, F. Haghighat, et al. Investigation of energy performance and operational schemes of a Tibet-focused PCM-integrated solar heating system employing a dynamic energy simulation model. *Energy* **172**:141–154, 2019. https://doi.org/10.1016/j.energy.2019.01.125

[4] S. R. Shamshirgaran, M. Khalaji Assadi, V. Badescu, H. H. Al-Kayiem. Upper limits for the work extraction by nanofluid-filled selective flat-plate solar collectors. *Energy* **160**:875–885, 2018. https://doi.org/10.1016/j.energy.2018.06.154

[5] N. E. Bassam, P. Maegaard, M. Schlichting. *Distributed renewable energies for off-grid communities*. Elsevier Science Publishing, Philadelphia, PA, 2012. https://doi.org/10.1016/C2011-0-07940-1

[6] Y. Tong, H. Lee, W. Kang, H. Cho. Energy and exergy comparison of a flat-plate solar collector using water, Al_2O_3 nanofluid, and CuO nanofluid. *Applied Thermal Engineering* **159**(113959):113959, 2019. https://doi.org/10.1016/j.applthermaleng.2019.113959

[7] M. Sadeghzadeh, M. H. Ahmadi, M. Kahani, et al. Smart modeling by using artificial intelligent techniques on thermal performance of flat-plate solar collector using nanofluid. *Energy Science & Engineering* **7**(5):1649–1658, 2019. https://doi.org/10.1002/ese3.381

[8] S. Choudhary, A. Sachdeva, P. Kumar. Investigation of the stability of MgO nanofluid and its effect on the thermal performance of flat plate solar collector. *Renewable Energy* **147**:1801–1814, 2020. https://doi.org/10.1016/j.renene.2019.09.126

[9] M. Moravej, M. V. Bozorg, Y. Guan, et al. Enhancing the efficiency of a symmetric flat-plate solar collector via the use of rutile TiO_2-water nanofluids. *Sustainable Energy Technologies and Assessments* **40**:100783, 2020. https://doi.org/10.1016/j.seta.2020.100783

[10] O. A. Hussein, K. Habib, A. S. Muhsan, et al. Thermal performance enhancement of a flat plate solar collector using hybrid nanofluid. *Solar Energy* **204**:208–222, 2020. https://doi.org/10.1016/j.solener.2020.04.034

[11] P. N. Nirmala. Comparative studies on efficiency of single and double glassed solar water heater. *Materials Today: Proceedings* **34**:420–424, 2021. https://doi.org/10.1016/j.matpr.2020.02.204

[12] F. Zarda, A. Hussein, S. Danook, B. Mohamad. Enhancement of thermal efficiency of nanofluid flows in a flat solar collector using CFD. *Diagnostyka* **23**(4):1–9, 2022. https://doi.org/10.29354/diag/156384

[13] A. Qashqaei, G. Asl. Numerical modeling and simulation of copper oxide nanofluids used in compact heat exchangers. *International Journal of Mechanical Engineering* **4**(2):1–8, 2015.

[14] E. C. Okonkwo, I. Wole-Osho, D. Kavaz, et al. Thermodynamic evaluation and optimization of a flat plate collector operating with alumina and iron mono and hybrid nanofluids. *Sustainable Energy Technologies and Assessments* **37**:100636, 2020. https://doi.org/10.1016/j.seta.2020.100636

[15] A. M. Alklaibi, L. S. Sundar, A. C. M. Sousa. Experimental analysis of exergy efficiency and entropy generation of diamond/water nanofluids flow in a thermosyphon flat plate solar collector. *International Communications in Heat and Mass Transfer* **120**:105057, 2021. https://doi.org/10.1016/j.icheatmasstransfer.2020.105057

[16] N. Akram, E. Montazer, S. N. Kazi, et al. Experimental investigations of the performance of a flat-plate solar collector using carbon and metal oxides based nanofluids. *Energy* **227**:120452, 2021. https://doi.org/10.1016/j.energy.2021.120452

[17] K. Farhana, K. Kadirgama, M. M. Noor, et al. CFD modelling of different properties of nanofluids in header and riser tube of flat plate solar collector. *IOP Conference Series: Materials Science and Engineering* **469**:012041, 2019. https://doi.org/10.1088/1757-899X/469/1/012041

[18] H. Hayder, M. Ali, A. M. Hussein, et al. Evaluation of shell and tube heat exchanger performance by using ZnO/Water nanofluids. *Journal of Harbin Institute Of Technology(New Series)* **2023**(6):62–69.

[19] S. Tarik Ahmed, H. Hayder Mohammed Ali. D theoretical study of the conventional and modified solar still. *The Iraqi Journal for Mechanical and Material Engineering* **20**(2):122–142, 2020. https://doi.org/10.32852/iqjfmme.v20i2.493

[20] Y. F. Nassar, K. A. Amer, H. J. El-Khozondar, et al. Thermoelectrical analysis of a new hybrid PV-thermal flat plate solar collector. In *2023 8th International Engineering Conference on Renewable Energy & Sustainability (ieCRES)*, pp. 1–5. IEEE, 2023. https://doi.org/10.1109/ieCRES57315.2023.10209472